Talanta 131 (2015) 475–479

Contents lists available at ScienceDirect

Talanta

journal homepage: www.elsevier.com/locate/talanta

A highly sensitive resonance light scattering probe for Alzheimer's amyloid-β peptide based on Fe_3O_4@Au composites

Ling Yu [a], Yintang Zhang [b], Ran Chen [c], Danhua Zhang [c], Xiuhua Wei [b], Fang Chen [b], Jianxiu Wang [a], Maotian Xu [a,b,*]

[a] College of Chemistry and Chemical Engineering, Central South University, Changsha 410083, PR China
[b] College of Chemistry and Chemical Engineering, Shangqiu Normal University, Shangqiu 476000, PR China
[c] College of Chemistry and Molecular Engineering, Zhengzhou University, Zhengzhou 450052, PR China

ARTICLE INFO

Article history:
Received 11 April 2014
Received in revised form
17 July 2014
Accepted 21 July 2014
Available online 11 August 2014

Keywords:
Amyloid-β peptide
Fe_3O_4@Au composites
Core/shell
Resonance light scattering

ABSTRACT

The fabrication of Fe_3O_4@Au composites as a novel resonance light scattering (RLS) probe for the sensitive detection of Alzheimer's amyloid-β peptide (Aβ) was demonstrated. Amino groups coated magnetic Fe_3O_4 nanoparticles were covered with gold shell by the classical Frens method. The resultant colloids were characterized with X-ray diffraction (XRD), transmission electron microscopy (TEM), X-ray photoelectron spectroscopy (XPS), dynamic light scattering (DLS) and UV–visible spectra. The results indicated that the composite particles with core/shell structure and an average diameter of ~320 nm were stable and biocompatible. The RLS intensity of Fe_3O_4@Au composites was significantly enhanced by interacting with Aβ. Under optimal conditions, good linear relationship between the ratio of RLS intensity I/I_0 at 463.0 nm and the logarithmic value of Aβ concentration in the range of 5.0×10^{-15}–5.56×10^{-9} M was found. The limit of detection (LOD) was 1.2×10^{-15} M. The proposed method is simple, sensitive and cost-effective and complementary to other existing methods for protein analysis.

1. Introduction

Alzheimer's disease (AD), the most common type of dementia in the elderly, is a progressive and devastating neurodegenerative disease causing memory loss, impaired thinking and other symptoms [1]. The hallmarks of AD pathology are extracellular amyloid-β peptide (Aβ) plaques and intracellular neurofibrillary tangles (NFT). Aβ is an ~4 kDa peptide consisting of 39–43 amino acid residues and derived from amyloid precursor protein (APP) [2]. In recent studies, Aβ indicates a biomarker for AD in cerebrospinal fluid (CSF), blood, plasma and serum [3–5]. Therefore, it is important to determine the Aβ concentration for early diagnosis and treatment of AD.

Many techniques have been developed for Aβ quantification, which include, but are not limited to, molecular spectroscopy (e.g., congo red staining [6], Fourier spectral analysis [7]), immunoassay (e.g., capillary isoelectric focusing immunoassay [8], enzyme-linked immunosorbent assay (ELISA) [9], immunoprecipitation [10], dot-blot [11] and western blot analysis [12]), molecular imaging (e.g., positron emission tomography (PET) [13] and fluorescence microscopy [14])), probe (e.g., small probe molecules [15] and quantum-dot nanoprobes [16]), electrochemical techniques [17,18], mass spectrometry (e.g., TOF-MS [19], MALDI-MS) [20]), chromatographic method (e.g., high performance liquid chromatography coupled with mass spectrometry (LC–MS) [21], capillary electrophoresis [22] and immobilized metal affinity chromatography [23]) and synthetic analysis method (e.g., meta-analysis [24]). However, each of these techniques has one or several undesirable limitations, such as expensive instrument, low sensitivity, and not environmental-friendly or instability of some reagents. Thus, it is important to develop alternative techniques which can be complementary to the existing techniques for specific applications.

Resonance light scattering (RLS) has emerged as a powerful optical technique based on elastic light-scattering [25]. Due to the advantages of high sensitivity, rapidness, simplicity and convenience (using a common spectrofluorometer), RLS has attracted much more attention from analytical chemists and physicists. Recently, RLS has been applied to determine inorganic ions [26,27], nanoparticles [28], proteins [29–31], nucleic acids [32,33], and so on.

Colloidal gold nanoparticles including different surface coatings have been investigated extensively to quantify protein concentrations. Enhanced RLS signal is often observed when the interaction between gold nanoparticles and protein molecules occurs as

* Corresponding author at: College of Chemistry and Chemical Engineering, Shangqiu Normal University, Shangqiu 476000, PR China. Tel.: +86 370 2594306.
E-mail addresses: xumaotian@163.com, xumaotian@sqnc.edu.cn (M. Xu).

http://dx.doi.org/10.1016/j.talanta.2014.07.067
0039-9140/

a result of the formation of aggregation or network structure of gold nanoparticles [34]. Detection of Aβ by spectroscopic techniques based on gold nanoparticles has been reported recently [35–38]. Wang and coworkers were the first to use gold nanoparticles as RLS probes to realize Aβ determination at level of ng/mL [36]. The blood Aβ levels in healthy and AD individuals are in the order of pg/mL [39]. Therefore, it is necessary to improve the RLS sensitivity based gold nanoparticles. To best of our knowledge, the RLS study of Fe_3O_4@Au composites has not been reported in the literature. The Fe_3O_4@Au composite particles possess the advantages of both colloid gold and magnetic particles, indicating that Fe_3O_4@Au composites can be a new approach to spectral RLS assay, and have numerous successful applications in the fields of biology and medicine [40–44].

In the present work, we report a highly sensitive probe based on Fe_3O_4@Au composites combined with RLS technique to determine the content of Alzheimer's β-amyloid peptide. Firstly, magnetic Fe_3O_4 nanoparticles are prepared. After amino groups coating, Fe_3O_4 nanoparticles are covered with gold shell by the classical Frens method. The resultant Fe_3O_4@Au composites are stable and biocompatible. The ratio of RLS intensity I/I_0 at 463.0 nm is taken to provide a distinguished sensitivity and satisfactory linear range for Aβ detection. Our approach is simple, sensitive and cost-effective in protein analysis.

2. Materials and methods

2.1. Materials and reagents

Aβ1–42 peptide (hereinafter to be referred as Aβ) was obtained from ChinaPeptides Co., Ltd. (Shanghai, China). Tetrachloroauric acid tetrahydrate ($HAuCl_4 \cdot 4H_2O$), iron (III) chloride hexahydrate ($FeCl_3 \cdot 6H_2O$), Sodium acetate anhydrous, ethylene glycol and ethanol were obtained from Sinopharm Chemical Reagent Co., Ltd. (Shanghai, China). Sodium citrate trihydrate ($Na_3C_6H_5O_7 \cdot 3H_2O$) was obtained from Amersco (USA). (3-Aminopropyl) triethoxysilane (APTES) was purchased from Sigma (USA). Hydrochloric acid (HCl) was purchased from Fangjing Chemical Reagent Co., Ltd. (Kaifeng, China). 1,1,1,3,3,3-Hexafluoro-2-propanol (HFIP) was obtained from Nanjing viochem Co., Ltd. (Nanjing, China). All chemicals were A.R. grade and used as received without any further purification. Millipore water (18.2 MΩ cm at 25 °C) was used throughout all experiments.

2.2. Preparation of amyloid-β peptide

Aβ was prepared as described previously [45]. Briefly, the lyophilized Aβ peptide was treated with HFIP at room temperature for 1 h in a sealed vial to dissolve potential aggregates. After that, HFIP was removed under a gentle stream of nitrogen and the peptide film was dissolved in DMSO to a concentration of 2 mM. Thus the peptide stock solutions were prepared.

2.3. Synthesis of Fe_3O_4 nanoparticles

Fe_3O_4 nanoparticles were prepared by hydrothermal treatment of $FeCl_3 \cdot 6H_2O$ and CH_3COONa in ethylene glycol solution. In a typical procedure, 0.2425 g $FeCl_3 \cdot 6H_2O$ was dissolved in 15 mL of ethylene glycol to form a clear solution, followed by the addition of 0.3751 g anhydrous CH_3COONa. The mixture was vigorously mixed by ultrasonication to give a homogeneous solution. Then the solution was transferred into a stainless steel autoclave (30 mL capacity) followed by hydrothermal treatment at 200 °C for 4.5 h. After the autoclave was cooled down to room temperature, the products were magnetically separated and washed several times with water and ethanol alternately to eliminate organic and inorganic impurities. After that, the products were dispersed in ethanol for further experiments.

2.4. Synthesis of Fe_3O_4@Au composites

To modify the surface of the magnetic nanoparticles with amino groups, Fe_3O_4 suspension (10 mg/mL, 2 mL) was added into 50 mL ethanol in a flask followed by the addition of 1 mL of APTES under stirring. The mixture was refluxed at 80 °C for 4 h. The APTES-coated Fe_3O_4 NPs were then magnetically separated, washed several times under sonication with water and ethanol and dispersed in ethanol.

Next, gold coating was implemented by the classical Frens method [46]. Briefly, 0.5 mL of APTES-coated Fe_3O_4 NPs (0.5 mg/mL) was added into 200 mL of 7.76 mM sodium citrate solution when the temperature was raised to 99 °C, followed by the dropwise addition of 10 mL of $HAuCl_4$ solution (10 mM) under a nitrogen atmosphere while stirring. The heating mantle was removed 30 min later. The solution was kept stirring for another 15 min and was cooled to room temperature.

The resulting dark particles were separated with a NdFeB magnet and washed with water several times. Uncoated Fe_3O_4 material was dissolved by a rinse with 30% HCl for more than 20 h, leaving largely pure Fe_3O_4@Au composites in the system [47].

2.5. Characterization of nanoparticle and composites

The phase structure was examined by powder X-ray diffraction (XRD), using X'Pert Pro MRD instrument (PANalytical B.V., Netherlands), with Cu Kα radiation at a scan rate of $0.033^\circ\ 2\theta\ s^{-1}$. Transmission electron microscopy (TEM) was obtained with Hitachi-800 instrument (Hitachi, Japan), operated at 120 kV. X-ray photoelectron spectroscopy (XPS) was measured on a K-Alpha 1063 Instrument (Thermo Fisher Scientific, UK). The size distribution of the microspheres was determined by Zetasizer Nano ZS (Malvern Instruments, UK). Ultraviolet–visible spectra were recorded using a Cary 60 spectrophotometer (Agilent technologies, USA) between 200 and 800 nm using a 1-cm path length quartz cuvette.

2.6. Resonance light scattering measurements

A certain amount of Fe_3O_4@Au dispersion was pipetted into a 1-cm path length quartz cuvette and diluted to 1 mL with H_2O, while the final concentration of Aβ varied from 5.0×10^{-15} to 5.56×10^{-9} M by successive addition of appropriate volume of Aβ (2.5 or 5 μL). The mixture was incubated for 10 min. Then RLS measurements were carried out using a Cary Eclipse fluorospectrophotometer (Agilent technologies, USA). The RLS intensities were recorded by synchronously scanning the excitation and emission monochromators ($\Delta\lambda = 0$ nm) between 200 and 800 nm. The excitation and emission slit width were both set to 5 nm. All the experiments were carried out at room temperature and repeated at least three times. The intensity was measured at 463.0 nm. The enhanced RLS intensity of Fe_3O_4@Au composites was termed as I/I_0 (I and I_0 were the RLS intensities of the systems with and without Aβ). In order to eliminate the effect of instrumental factors on the light scattering measurement, the scattering intensities were corrected by using the reported correction methods [48]. Briefly, corrected RLS intensities were calculated by division of the signal intensity at the wavelength by the corresponding source intensity. Meanwhile, the scattering intensities were also corrected for dilution effect.

3. Results and discussion

3.1. Characterization of Fe_3O_4@Au composites

Fig. 1 shows the XRD patterns of the prepared Fe_3O_4 NPs and Fe_3O_4@Au composites. In curve (a) for Fe_3O_4, the diffraction peaks can be assigned to the cubic structure of Fe_3O_4 crystal according to JCPDS card no. 19-0629. In curve (b) for Fe_3O_4@Au, the shape peaks are consistent with that of Au nanocrystal (JCPDS card no. 04-0784). No peak was found for Fe_3O_4 due to the heavy atom effect of Au indicating complete coverage of the Fe_3O_4 core by Au shell [49], which is consistent with previous reports [50].

The morphology of the as-synthesized particles was investigated by TEM. Fig. S1 (Supporting information, SI) shows the typical TEM images of Fe_3O_4 NPs (A) with a diameter of ~156 nm and Fe_3O_4@Au composites (B) with a diameter of ~320 nm. It can be seen from Fig. S1A that the Fe_3O_4 NPs are of well spherical structure with relatively smooth surfaces. After coating with amine groups, gold was then deposited onto the surface of amine-coated Fe_3O_4 NPs. The diameter of Fe_3O_4@Au composites increases, as shown in Fig. S1B, which is twice as large as that of Fe_3O_4 NPs. However, the thickness of gold shells on the surface of Fe_3O_4 NPs was determined to be only approximate 9 nm, suggesting that Fe_3O_4 clusters may exist inside a single Fe_3O_4@Au composite [50].

The size distribution of Fe_3O_4@Au composites was determined by dynamic light scattering (DLS). Fig. S2 shows that the average hydrodynamic diameter of Fe_3O_4@Au composites is 337 nm, in good agreement with the TEM results.

XPS results of Fe_3O_4@Au composites are shown in Fig. 2. Two characteristic peaks of Au 4f5/2 and Au 4f7/2, positioned at 83.3 eV and 87.0 eV, respectively, are clearly observed in Fig. 2B, while no Auger peaks of Fe are found (Fig. 2A), indicating that the Fe_3O_4@Au composite surface is mainly composed of gold with a thickness of more than 5 nm [51].

UV–vis spectrum of Fe_3O_4@Au composites is shown in Fig. 3A. The absorption peak of Fe_3O_4@Au composites was red-shifted to 546 nm compared with that of colloid gold at 529 nm. The reason for this might be that the composite diameter is much larger than that of colloid gold [47]. When the Fe_3O_4@Au dispersion was exposed to the external magnetic field for 2 min, no obvious colloid gold were detected in the supernatant, indicating that not pure gold nanoparticles but magnetic Fe_3O_4 particles existed in the as-prepared Fe_3O_4@Au composites. Furthermore, as can be seen in Fig. 3B, Fe_3O_4@Au composites have scattering characteristic peaks of both Fe_3O_4 and colloid gold. These results are a further proof of core/shell structure of the Fe_3O_4@Au composites.

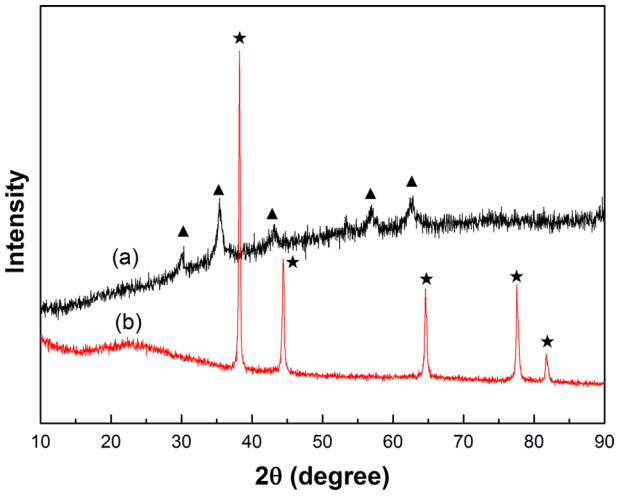

Fig. 1. XRD patterns of (a) Fe_3O_4 NPs and (b) Fe_3O_4@Au hybrid composites. ▲ shows the diffraction peaks of Fe_3O_4 and ★ shows the diffraction peaks of gold.

3.2. Spectral characteristics

The RLS spectra of Aβ (1), water (2), Fe_3O_4@Au composite (3) and Aβ-Fe_3O_4@Au composite (4) are shown in Fig. S3. It can be seen that both Aβ and Fe_3O_4@Au composite have weak scattering signal. When Aβ is mixed with Fe_3O_4@Au composite, the RLS signal is remarkably enhanced with two obvious peaks at 408.0 nm and 463.0 nm. The RLS intensity of the system reaches its maximum at 463.0 nm. Hence, 463.0 nm was selected as the determination wavelength.

3.3. Possible reasons for RLS enhancement

According to the RLS theory [25], the RLS intensity is proportional to r^6 where r is the radius of the particle. However, too larger particle size is not recommended due to its instability. The average diameter of Fe_3O_4@Au composites is ~320 nm, which is much greater than 1/20 of the wavelength of incident light. Therefore, the light scattering of Fe_3O_4@Au composites can be considered as the Mie scattering rather than the Rayleigh scattering. According to the Mie scattering theory, the RLS properties have close relationship with the molecular volume and morphology of the particles [52]. The bigger the molecular volume, the higher the RLS intensity can be obtained.

Once the Fe_3O_4@Au composites are exposed to Aβ molecules, Aβ is believed to bind to the surface of gold shell via both the apolar and the N-donors containing side-chains of amino acids [53]. The formation of conjugates of Fe_3O_4@Au-Aβ results in increasing the size of scatters. Therefore, the RLS intensity of the system is enhanced.

It should be noted that the Mie scattering can be affected by small magnetic spheres magnetism, called as the Magnetic Mie scattering, and the magnetization of small clusters of radius larger than 10 nm is size dependent [54]. However, the mechanism of the effect of magnetic Fe_3O_4 core on the RLS remains unclear.

3.4. Effect of pH and buffer

The surrounding matrix may greatly affect the scattering spectrum of particles. The effects of pH and type of buffer were investigated. As can be seen in Fig. S4(1A) and (1B), the maximum RLS peak wavelengths varies with pH values. When pH value decreases, negatively charged Au particles covered with citrate have the tendency to form aggregation because the electrostatic repellency among Au particles becomes weak. As a result, the maximum RLS peak redshift happens. When pH is in the range of 6.80–7.96, the RLS intensities at the maximum RLS peak wavelengths were much smaller than with other pH values indicating lower background determination. However, the RLS signals were not so stable along with the time. Thus, the effects of different buffer with similar pH values including HEPES buffer, Tris–HCl buffer (Tris) and Brittion–Robinson buffer (BR) together with H_2O were investigated. It can be seen from Fig. S4(2B) that the RLS intensity in H_2O keeps very stable and is also small. The results indicated that high ionic strength was the possible reason for RLS instability [55]. Therefore, H_2O is chosen for further research.

3.5. The incubation time and stability

The effect of time of the RLS intensity of the composite–Aβ system was studied. The results showed that the reaction between Fe_3O_4@Au composite and Aβ occurred rapidly at room temperature

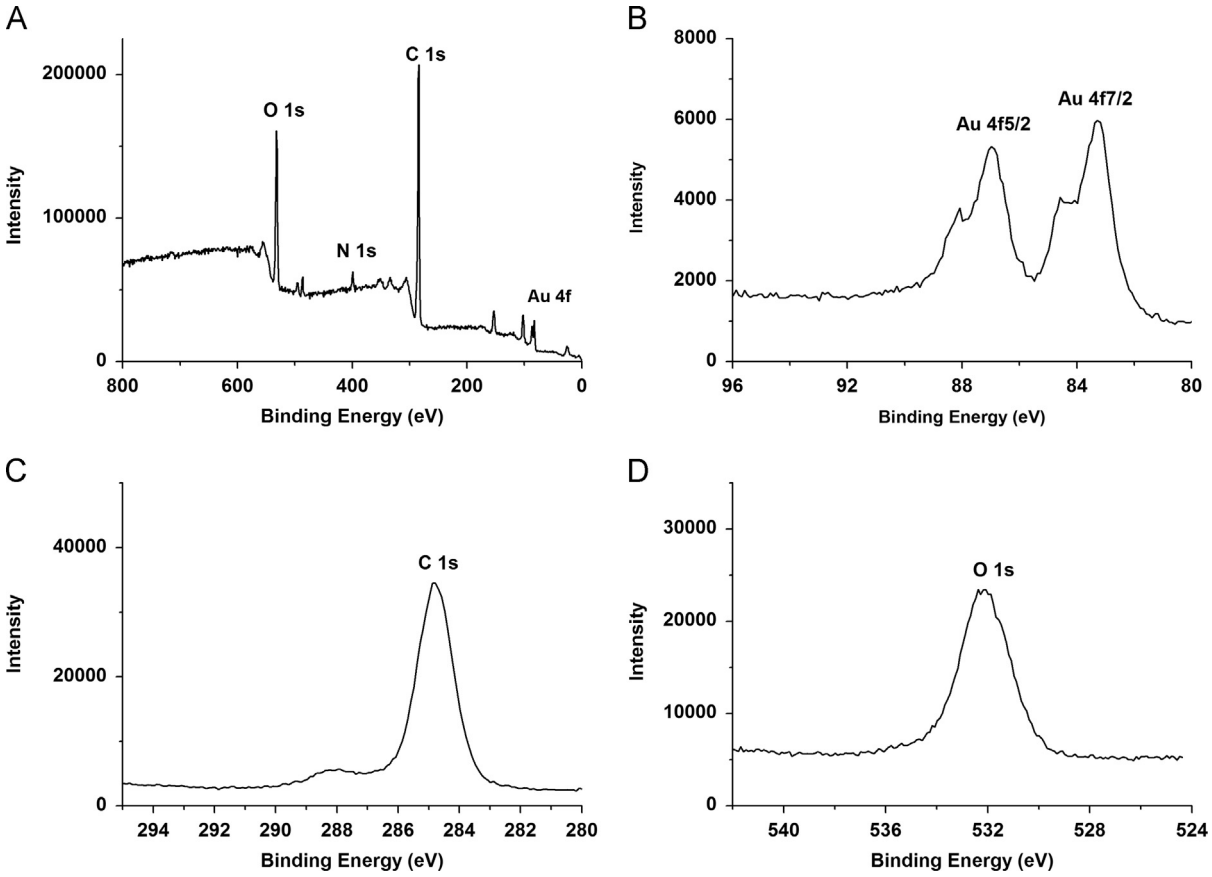

Fig. 2. XPS spectra of Fe_3O_4@Au composites.

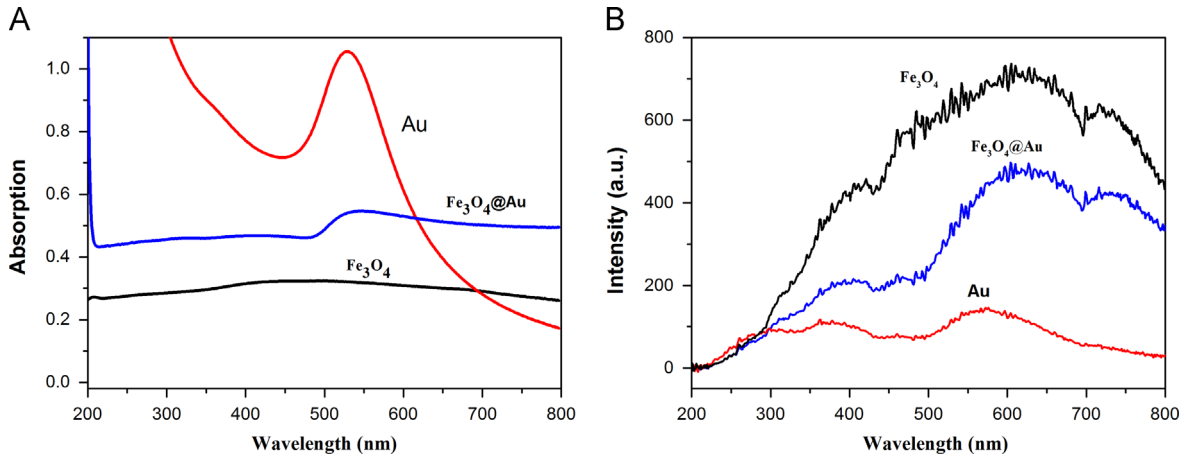

Fig. 3. UV–vis (A) and RLS (B) spectra of Fe_3O_4, colloid gold and Fe_3O_4@Au composites.

(< 10 min). The scattering intensity is stable for at least 60 min. Thus, 10 min of incubation time was considered. The assay exhibits good stability and can be used for practical determination of Aβ.

3.6. Analytical performance

Under the optimal conditions, the dependence of the RLS intensity on the concentration of Aβ was determined. As shown in Fig. 4, the RLS intensity increases with the increase of Aβ concentration. There is a good linear relationship between the ratio of RLS intensity I/I_0 and the logarithmic value of Aβ concentration in the range of 5.0×10^{-15}–5.56×10^{-9} M (the inset in Fig. 4), and the linear regression equation is $I/I_0 = 24.77 + 1.65 \log C$ (M) with the correlation coefficient R^2 0.986.The limit of detection (LOD) is calculated to be 1.2×10^{-15} M. Each concentration was repeated at least three times and the relative standard deviations (RSD) are between 2.2% and 13.8%. The proposed RLS approach exhibits sufficient low detection level and significant wide linear range, and compares well with other Aβ assays [36–38]. Meanwhile, the detection limit is far lower than that of the present commercial $A\beta_{1-42}$ ELISA kit (in the order of a few to a few hundred pg/mL or pM).

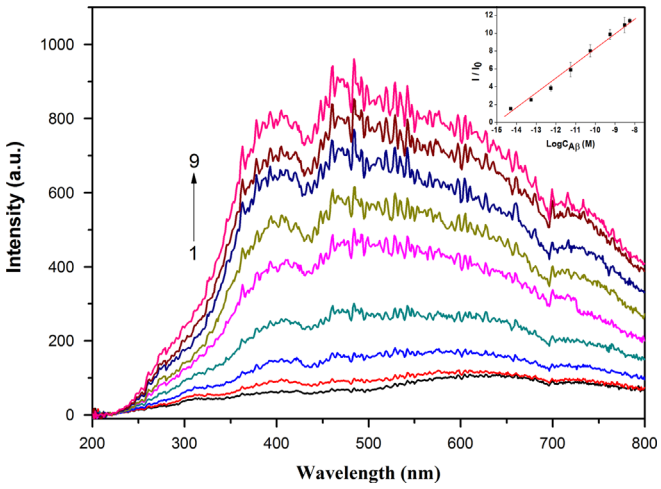

Fig. 4. The RLS spectra of Fe_3O_4@Au composites in the presence of different concentration of Aβ. c (Fe_3O_4@Au composite)=0.2 mg/mL; C (Aβ)/(10^{-12} M), 1–9: 0, 0.005, 0.055, 0.56, 5.56, 55.6, 556, 3056 and 5556. Inset: the linear relationship corresponding to the ratio of RLS intensity I/I_0 at 463.0 nm vs. logarithmic value of Aβ concentration. Each concentration was repeated at least three times.

4. Conclusions

We have demonstrated the fabrication of Fe_3O_4@Au composites as a RLS probe for the sensitive detection of Alzheimer's Aβ. The resultant composite has an average diameter of ~320 nm. The Fe_3O_4 core was completely covered by Au shell with a thickness of ~9 nm. The RLS signal intensity of Fe_3O_4@Au was enhanced by interacting with Aβ. Under optimal conditions, the ratio of RLS intensity I/I_0 at 463.0 nm is proportional to the logarithmic value of Aβ concentration in the range of 5.0×10^{-15}–5.56×10^{-9} M. The detection limit is as low as 1.2×10^{-15} M. The discrimination for the structural diversity of Aβ, e.g. monomers, oligomers, and even fibrils, is still under study. Our approach has proved to be simple, sensitive, label-free and cost-effective. The proposed method is complementary to other existing methods for protein analysis.

Acknowledgments

We gratefully acknowledge partial support of this work by the National Natural Science Foundation of China (Nos. 20905045, 21175091), the Program for Innovative Research Team (in Science and Technology) in University of Henan Province (No. 2012IRTSTHN018), the Innovation Scientists and Technicians Troop Construction Projects of Henan Province, the Science and Technique Foundation of Henan province (Nos. 102102310385, 1121023-10217) and the Foundation for University Young Key Teacher Program of Henan Province (No. 2012GGJS-168).

Appendix A. Supporting information

Supplementary data associated with this article can be found in the online version at http://dx.doi.org/10.1016/j.talanta.2014.07.067.

References

[1] M.R. Boyd, Alzheimer's Disease Diagnosis and Treatments, Nova Science, Hauppauge, N.Y., 2011.
[2] Q.M. Wang, N. Shah, J. Zhao, C.S. Wang, C. Zhao, L.Y. Liu, L.Y. Li, F.M. Zhou, J. Zheng, Phys. Chem. Chem. Phys. 13 (2011) 15200–15210.
[3] N.S.M. Schoonenboom, Y.A.L. Pijnenburg, C. Mulder, S.M. Rosso, E.J. Van Elk, G.J. Van Kamp, J.C. Van Swieten, P. Scheltens, Neurology 62 (2004) 1580–1584.
[4] P.D. Mehta, Curr. Alzheimer Res. 4 (2007) 359–363.
[5] H. Hampel, Y. Shen, D.M. Walsh, P. Aisen, L.M. Shaw, H. Zetterberg, J.Q. Trojanowski, K. Blennow, Exp. Neurol. 223 (2010) 334–346.
[6] W.E. Klunk, R.F. Jacob, R.P. Mason, Anal. Biochem. 266 (1999) 66–76.
[7] R.A. Armstrong, N.J. Cairns, Neuropathol. Appl. Neurobiol. 36 (2010) 248–257.
[8] U. Haussmann, O. Jahn, P. Linning, C. Janssen, T. Liepold, E. Portelius, H. Zetterberg, C. Bauer, J. Schuchhardt, H.J. Knolker, H. Klafki, J. Wiltfang, Anal. Chem. 85 (2013) 8142–8149.
[9] M. Jensen, T. Hartmann, B. Engvall, R. Wang, S.N. Uljon, K. Sennvik, J. Naslund, F. Muehlhauser, C. Nordstedt, K. Beyreuther, L. Lannfelt, Mol. Med. 6 (2000) 291–302.
[10] E. Portelius, A. Westman-Brinkmalm, H. Zetterberg, K. Blennow, J. Proteome Res. 5 (2006) 1010–1016.
[11] C.K. Wang, D.J. Liu, Z.X. Wang, Chem. Commun. 48 (2012) 8392–8394.
[12] A. Potempska, K. Mack, P. Mehta, K.S. Kim, D.L. Miller, Amyloid—Int. J. Exp. Clin. Investig. 6 (1999) 14–21.
[13] C. Hommet, K. Mondon, V. Camus, M.J. Ribeiro, E. Beaufils, N. Arlicot, P. Corcia, M. Paccalin, F. Minier, T. Gosselin, G. Page, D. Guilloteau, S. Chalon, Dement. Geriatr. Cogn. 37 (2014) 1–18.
[14] P.T. Chang, Y. Su, Brain Res. Protoc. 6 (2000) 6–12.
[15] H.B. Hong, I.H. Nam, S.W. Sohn, K.B. Song, J. Biomed. Nanotechnol. 9 (2013) 1088–1091.
[16] K. Tokuraku, M. Marquardt, T. Ikezu, PLoS One 4 (2009) 11.
[17] L. Liu, F. Zhao, F.J. Ma, L.P. Zhang, S.L. Yang, N. Xia, Biosens. Bioelectron. 49 (2013) 231–235.
[18] J.V. Rushworth, A. Ahmed, H.H. Griffiths, N.M. Pollock, N.M. Hooper, P.A. Millner, Biosens. Bioelectron. 56 (2014) 83–90.
[19] A. Matsumoto, R. Matsumoto, K. Kadoyama, T. Nishimoto, S. Matsuyama, O. Midorikawa, Int. J. Pept. Res. Ther. 15 (2009) 205–210.
[20] S. Trimpin, M.L. Deinzer, J. Am. Soc. Mass Spectrom. 18 (2007) 1533–1543.
[21] K. Matsumiya, J. Kamiie, S. Ohtsuki, T. Terasaki, Drug Metab. Rev. 39 (2007) 59–60.
[22] R. Verpillot, H. Esselmann, M.R. Mohamadi, H. Klafki, F. Poirier, S. Lehnert, M. Otto, J. Wiltfang, J.L. Viovy, M. Taverna, Anal. Chem. 83 (2011) 1696–1703.
[23] A.H. Simonsen, S.F. Hansson, U. Ruetschi, J. McGuire, V.N. Podust, H.A. Davies, P. Mehta, G. Waldemar, H. Zetterberg, N. Andreasen, A. Wallin, K. Blennow, Dement. Geriatr. Cogn. 23 (2007) 246–250.
[24] F. Song, A. Poljak, M. Valenzuela, R. Mayeux, G.A. Smythe, P.S. Sachdev, J. Alzheimers Dis. 26 (2011) 365–375.
[25] R.F. Pasternack, C. Bustamante, P.J. Collings, A. Giannetto, E.J. Gibbs, J. Am. Chem. Soc. 115 (1993) 5393–5399.
[26] H. Cao, M. Wei, Z. Chen, Y. Huang, Analyst 138 (2013) 2420–2426.
[27] Y. Wang, K. Tan, R. Yuan, Acta Chim. Sin. 70 (2012) 643–648.
[28] J. Zhu, Y.C. Wang, L.Q. Huang, Y.M. Lu, Phys. Lett. A 323 (2004) 455–459.
[29] Z. Chen, J. Liu, Y. Han, Talanta 71 (2007) 1246–1251.
[30] B. Gu, H. Zhong, X.M. Li, Y.Z. Wang, B.C. Ding, Z.P. Cheng, L.L. Zhang, S.P. Li, C. Yao, J. Appl. Spectrosc. 80 (2013) 486–491.
[31] Q.E. Cao, Z.T. Ding, R.B. Fang, X. Zhao, Analyst 126 (2001) 1444–1448.
[32] W.J. Zhang, H.P. Xu, S.Q. Wu, X.G. Chen, Z.D. Hu, Analyst 126 (2001) 513–517.
[33] Q. Zou, Q. Yan, G. Song, S. Zhang, L. Wu, Biosens. Bioelectron. 22 (2007) 1461–1465.
[34] G. Weng, J. Li, J. Zhu, J. Zhao, Colloids Surf. A 369 (2010) 253–259.
[35] C.K. Wang, J.E. Wang, D.J. Liu, Z.X. Wang, Talanta 80 (2010) 1626–1631.
[36] C. Wang, D. Liu, Z. Wang, Chem. Commun. 47 (2011) 9339–9341.
[37] W.A. El-Said, T.H. Kim, C.H. Yea, H. Kim, J.W. Choi, J. Nanosci. Nanotechnol. 11 (2011) 768–772.
[38] M. Sakono, T. Zako, M. Maeda, Anal. Sci. 28 (2012) 73–76.
[39] A. Ruiz, P. Pesini, A. Espinosa, V. Pérez-Grijalba, S. Valero, O. Sotolongo-Grau, M. Alegret, I. Monleón, A. Lafuente, M. Buendía, M. Ibarria, S. Ruiz, I. Hernández, I. San José, L. Tárraga, M. Boada, M. Sarasa, Plos One 8 (2013) e81334.
[40] H. Yin, C. Wang, H. Zhu, S.H. Overbury, S. Sun, S. Dai, Chem. Commun. (2008) 4357–4359.
[41] C. Yang, J. Wu, Y. Hou, Chem. Commun. 47 (2011) 5130–5141.
[42] G.K. Kouassi, Curr. Nanosci. 7 (2011) 510–523.
[43] K.C.F. Leung, S. Xuan, X. Zhu, D. Wang, C.P. Chak, S.F. Lee, W.K.W. Ho, B.C. T. Chung, Chem. Soc. Rev. 41 (2012) 1911–1928.
[44] Y.H. Bai, J.Y. Li, J.J. Xu, H.Y. Chen, Analyst 135 (2010) 1672–1679.
[45] D. Brambilla, R. Verpillot, M. Taverna, L. De Kimpe, B. Le Droumaguet, J. Nicolas, M. Canovi, M. Gobbi, F. Mantegazza, M. Salmona, V. Nicolas, W. Scheper, P. Couvreur, K. Andrieux, Anal. Chem. 82 (2010) 10083–10089.
[46] G. Frens, Nat. Phys. Sci. 241 (1973) 20–22.
[47] Y.L. Cui, W.L. Hui, J. Su, Y.N. Wang, C. Chen, Sci. China Ser. B 48 (2005) 273–278.
[48] P. McPhie, Anal. Biochem. 348 (2006) 157–159.
[49] Z. Xu, Y. Hou, S. Sun, J. Am. Chem. Soc. 129 (2007) 8698–8699.
[50] X. Zhou, W. Xu, Y. Wang, Q. Kuang, Y. Shi, L. Zhong, Q. Zhang, J. Phys. Chem. C 114 (2010) 19607–19613.
[51] K. Siegbahn, Philos. Trans. R. Soc. Lond., Ser. A 268 (1970) 33–57.
[52] W. Hergert, T. Wriedt, The Mie Theory: Basics and Applications, Springer, Berlin, 2012.
[53] A. Majzik, L. Fülöp, E. Csapó, F. Bogár, T. Martinek, B. Penke, G. Bíró, I. Dékány, Colloids Surf. B 81 (2010) 235–241.
[54] R.J. Tarento, K.H. Bennemann, P. Joyes, J. Van de Walle, Phys. Rev. E 69 (2004) 5.
[55] J.K. Lim, S.A. Majetich, R.D. Tilton, Langmuir 25 (2009) 13384–13393.